

# On the influence of wind on extreme wave events

J. Touboul

Institut de Recherche sur les Phénomènes Hors Equilibre, Marseille, France

Received: 19 October 2006 – Revised: 8 January 2007 – Accepted: 8 January 2007 – Published: 25 January 2007

**Abstract.** This work studies the impact of wind on extreme wave events, by means of numerical analysis. A High Order Spectral Method (HOSM) is used to generate freak, or rogue waves, on the basis of modulational instability. Wave fields considered here are chosen to be unstable to two kinds of perturbations. The evolution of components during the propagation of the wave fields is presented. Their evolution under the action of wind, modeled through Jeffreys' sheltering mechanism, is investigated and compared to the results without wind. It is found that wind sustains rogue waves. The perturbation most influenced by wind is not necessarily the most unstable.

## 1 Introduction

Extreme waves events, called rogue, or freak waves, are well known from the seafarers. Historically believed to belong to the domain of myth, more than to the domain of physics, they are now widely observed and witnessed. A large number of disasters have been reported by Mallory (1974) and Lawton (2001). This phenomenon has been observed in various conditions, and various places. It points out that a large number of physical mechanisms is involved in the generation of freak waves. A large review of the different mechanisms involved can be found in Kharif and Pelinovsky (2003). Up to now, there is no definitive consensus about their definition. The definition based on height is often used. A wave is considered to be rogue when its height exceeds twice the significant wave height of the wave field.

These waves often occur in storm areas, in presence of strong wind. In those areas,  $H_s$  is generally large, leading freak waves defined by  $H \geq 2 \times H_s$  to be very devastating. This observation lead to wonder what can be the impact of wind on such waves. Recent work by Touboul et al. (2006) and Giovanangeli et al. (2006) pointed out experimentally

and numerically that freak waves generated by means of dispersive focusing were sustained by wind. A focusing wave train was emitted, and propagated under the action of wind. It was found that the freak wave was shifted, and had a higher lifetime. Part of those results were observed numerically by modeling the wind action through Jeffreys' sheltering mechanism (Jeffreys, 1925).

Thus, one can wonder if these characteristics are generic for freak waves in general, or are specific to the case of dispersive focusing. Previous experimental work by Bliven et al. (1986), comforted by theoretical results by Trulsen and Dysthe (1991) observed that wind action was to delay, or even to suppress Benjamin-Feir instability. But more recent work by Banner and Tian (1998) concluded that this result could be different, with another approach for wind modeling. Very recent work by Touboul and Kharif (2006) showed that the Jeffreys' sheltering model was leading to an increase of the lifetime of the freak wave due to modulational instability, observing the results found in the case of dispersive focusing. However, the authors concluded that the underlying physics of both cases were different. As a matter of fact, it is interesting to investigate further the present phenomenon.

Following this purpose, the approach used here is designed to analyze the evolution of several perturbations under the action of wind. The numerical scheme introduced by Domermuth and Yue (1987) and West et al. (1987) is presented first. Nonlinear equations of waves propagation are solved by means of a High Order Spectral Method (HOSM). It is based on the pseudo-spectral treatment of the equations, resulting in a quite good precision, given the high efficiency of the method. This approach allows to simulate long time evolution (several hundreds of peak period) of the wave field to model Benjamin-Feir instability with a good accuracy. The model is presented in Sect. 2. Wind modeling is also presented in this section, explaining how Jeffreys' sheltering mechanism can be introduced in the equations of wave propagation. In Sect. 3, the initial conditions used in the numerical experiences are detailed, and results are presented and discussed in Sect. 4.

Correspondence to: J. Touboul  
(julien.touboul@irphe.univ-mrs.fr)

## 2 Modeling of the problem

### 2.1 Governing equations of the fluid

The fluid is assumed to be inviscid and the motion irrotational, so that the velocity  $\mathbf{u}$  may be expressed as the gradient of a potential  $\phi(x, z, t)$ :  $\mathbf{u}=\nabla\phi$ . If the fluid is assumed to be incompressible, the governing equation in the fluid is the Laplace's equation  $\Delta\phi=0$ .

The waves are supposed to propagate in infinite depth, and the fluid should remain asymptotically unperturbed by waves motion. Thus, the bottom condition writes

$$\nabla\phi \rightarrow 0 \quad \text{when } z \rightarrow -\infty. \quad (1)$$

The kinematic definition of the sea surface, which expresses the fact that a particle of the surface should remain on it, is expressed by

$$\frac{\partial\eta}{\partial t} + \frac{\partial\phi}{\partial x} \frac{\partial\eta}{\partial x} - \frac{\partial\phi}{\partial z} = 0 \quad \text{on } z = \eta(x, t). \quad (2)$$

Since surface tension effects are ignored, the dynamic boundary condition which corresponds to pressure continuity through the interface, can be written

$$\frac{\partial\phi}{\partial t} + \frac{(\nabla\phi)^2}{2} + g\eta + \frac{p_a}{\rho_w} = 0 \quad \text{on } z = \eta(x, t). \quad (3)$$

where  $g$  is the gravitational acceleration,  $p_a$  the pressure at the sea surface and  $\rho_w$  the density of water. The atmospheric pressure at the sea surface can vary in space and time.

By introducing the potential velocity at the free surface  $\phi^s(x, t)=\phi(x, \eta(x, t), t)$ , Eqs. (2) and (3) writes

$$\frac{\partial\phi^s}{\partial t} = -\eta - \frac{(\nabla\phi^s)^2}{2} + \frac{1}{2}W^2[1 + (\nabla\eta)^2] - p. \quad (4)$$

$$\frac{\partial\eta}{\partial t} = -\nabla\phi^s \cdot \nabla\eta + W[1 + (\nabla\eta)^2]. \quad (5)$$

where  $p$  is the nondimensional form of  $p_a$ , and where

$$W = \frac{\partial\phi}{\partial z}(x, \eta(x, t), t). \quad (6)$$

Equations (4) and (5) are given in dimensionless form. Reference length, reference velocity and reference pressure are,  $1/k_0$ ,  $\sqrt{g/k_0}$  and  $\rho_w g/k_0$  respectively.

The numerical method used to solve the evolution equations is based on a pseudo-spectral treatment with an explicit fourth-order Runge-Kutta integrator with constant time step, similar to the method developed by Dommermuth and Yue (1987). More details, and test reports of the method can be found in Skandrani et al. (1996).

### 2.2 The Jeffreys' sheltering mechanism

Previous works on rogue waves have not considered the direct effect of wind on their dynamics. It was assumed that they occur independently of wind action, that is far away from storm areas where wind wave fields are formed. Herein the Jeffreys' theory (see Jeffreys, 1925) is invoked for the modelling of the pressure,  $p_a$ . Jeffreys suggested that the energy transfer was due to the form drag associated with the flow separation occurring on the leeward side of the crests. The air flow separation would cause a pressure asymmetry with respect to the wave crest resulting in a wave growth. This mechanism can be invoked only if the waves are sufficiently steep to produce air flow separation. Banner and Melville (1976) have shown that separation occurs over near breaking waves. For weak or moderate steepness of the waves this phenomenon cannot apply and the Jeffreys' sheltering mechanism becomes irrelevant.

Following Jeffreys (1925), the pressure at the interface  $z=\eta(x, t)$  is related to the local wave slope according to the following expression

$$p_a = \rho_a s (U - c)^2 \frac{\partial\eta}{\partial x}. \quad (7)$$

where the constant,  $s$  is termed the sheltering coefficient,  $U$  is the wind speed,  $c$  is the wave phase velocity and  $\rho_a$  is atmospheric density. The sheltering coefficient,  $s=0.5$ , has been calculated from experimental data. In a nondimensional form, Eq. (7) rewrites

$$p = \frac{\rho_a}{\rho_w} s \left(\frac{U}{c} - 1\right)^2 \frac{\partial\eta}{\partial x}. \quad (8)$$

In order to apply the relation (8) for only very steep waves we introduce a threshold value for the slope  $(\partial\eta/\partial x)_c$ . When the local slope of the waves becomes larger than this critical value, the pressure is given by Eq. (7) otherwise the pressure at the interface is taken equal to a constant which is chosen equal to zero without loss of generality. This means that wind forcing is applied locally in time and space.

In the following simulations, parameter  $(\partial\eta/\partial x)_c$  has been taken equal to 0.32. This parameter is chosen arbitrarily, noticing that this slope corresponds to an angle close to  $30^\circ$ , which the angle of the limiting Stokes wave in infinite depth. The parameter  $\frac{U}{c}$  has been taken equal to 1.6, which would correspond to a wind speed  $U=25$  m/s for waves of period  $T=10$  s.

## 3 Initialization of the method

Stokes waves are well known to be unstable to the Benjamin-Feir instability, or modulational instability. It is the consequence of the resonant interaction of four components presents in the wave field. This instability corresponds to a quartet interaction between the fundamental component  $k_0$  counted twice and two satellites  $k_1=k_0(1 + p)$  and

$k_2=k_0(1-p)$  where  $p$  is the wavenumber of the modulation. Instability occurs when the following resonance conditions are fulfilled.

$$k_1 + k_2 = 2k_0 \quad \text{and} \quad \omega_1 + \omega_2 = 2\omega_0. \quad (9)$$

where  $\omega_i$  with  $i=0, 1, 2$  are frequencies of the carrier and satellites. A presentation of the different classes of instability of Stokes waves is given in the review paper by Dias and Kharif (1999).

The procedure used to calculate the linear stability of Stokes waves is similar to the method described by Kharif and Ramamonjariisoa (1988). Let  $\eta=\bar{\eta}+\eta'$  and  $\phi=\bar{\phi}+\phi'$  be the perturbed elevation and perturbed velocity potential.  $(\bar{\eta}, \bar{\phi})$  and  $(\eta', \phi')$  correspond respectively to the unperturbed Stokes wave and to the infinitesimal perturbative motion ( $\eta' \ll \bar{\eta}, \phi' \ll \bar{\phi}$ ). Following Longuet-Higgins (1985), the Stokes wave of amplitude  $a_0$  and wavenumber  $k_0$  is computed iteratively, providing a very high order solution of  $(\bar{\eta}, \bar{\phi})$ . This decomposition is introduced in the boundary conditions (4) and (5) linearized about the unperturbed motion, and the following form is used:

$$\eta' = \exp(\lambda t + i p x) \sum_{-\infty}^{\infty} a_j \exp(i j x). \quad (10)$$

$$\phi' = \exp(\lambda t + i p x) \sum_{-\infty}^{\infty} b_j \exp(i j x + \gamma_j z). \quad (11)$$

where  $\lambda, a_j$  and  $b_j$  are complex numbers and where  $\gamma_j = |p+j|$ . An eigenvalue problem for  $\lambda$  with eigenvector  $\mathbf{u}=(\mathbf{a}_j, \mathbf{b}_j)^t: (\mathbf{A}-\lambda\mathbf{B})\mathbf{u}=\mathbf{0}$  is obtained, where  $\mathbf{A}$  and  $\mathbf{B}$  are complex matrices depending on the unperturbed wave steepness of the basic wave. The physical disturbances are obtained from the real part of the complex expressions  $\eta'$  and  $\phi'$  at  $t=0$ .

McLean et al. (1981) and McLean (1982) showed that the dominant instability of a uniformly-traveling train of Stokes' waves in deep water is the two-dimensional modulational instability, or class I instability, as soon as its steepness is less than  $\epsilon=0.30$ .

In the following simulations, two initial conditions are used. Those conditions are designed to lead to modulational instability. The first one, named initial condition (1), is a Stokes wave of steepness  $\epsilon=0.11$ , disturbed by its most unstable perturbation which corresponds to  $p \approx 2/9 \approx 0.22$ . The fundamental wave number of the Stokes wave is  $k_0=9$  and the dominant sidebands are  $k_1=7$  and  $k_2=11$  for the subharmonic and the superharmonic part of the perturbation respectively.

The initial condition (2), is also a Stokes wave of same steepness, disturbed by its most unstable perturbation  $p \approx 2/9 \approx 0.22$ . But the linear stability analysis demonstrates that the Stokes of  $\epsilon=0.11$  is also unstable to the perturbation  $q \approx 1/9 \approx 0.11$ , which is added to the previous initial condition. Thus, the fundamental wave number of the Stokes wave

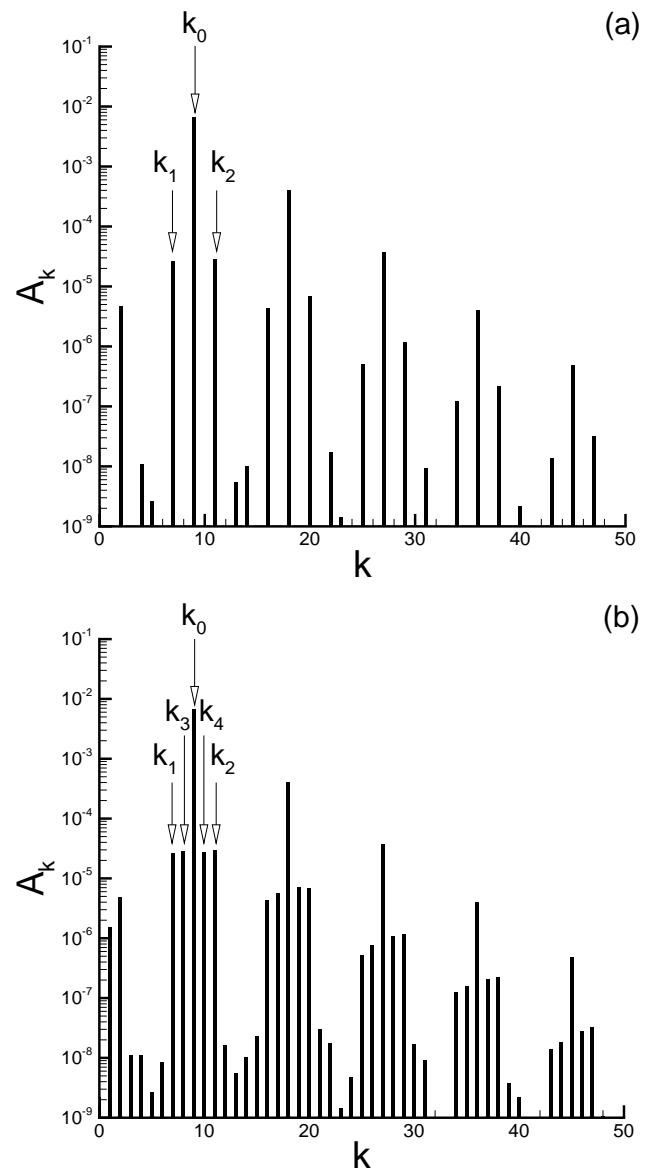


**Fig. 1.** Spectra of the two initial conditions used in the simulations. (a): initial condition (1), with perturbation  $p$  alone; (b): initial condition (2), with both perturbations  $p$  and  $q$ . Spectra are presented up to  $k=50$  for sake of clarity.

is still  $k_0=9$  and the sidebands  $k_3=8$  and  $k_4=10$  for subharmonic and superharmonic part of the modulation  $q$  are also present, and have the same amplitude than sidebands  $k_1=7$  and  $k_2=11$  corresponding to the modulation  $p$ .

Higher harmonics are present in the interaction but they are not presented here, for sake of clarity. Figure 1 present the spectra of these initial conditions, up to fourth harmonic. From this figure, it also appears that wavenumbers  $k=1$  and  $k=2$  are present. They respectively correspond to the wavenumbers of the perturbations  $p$  and  $q$ .

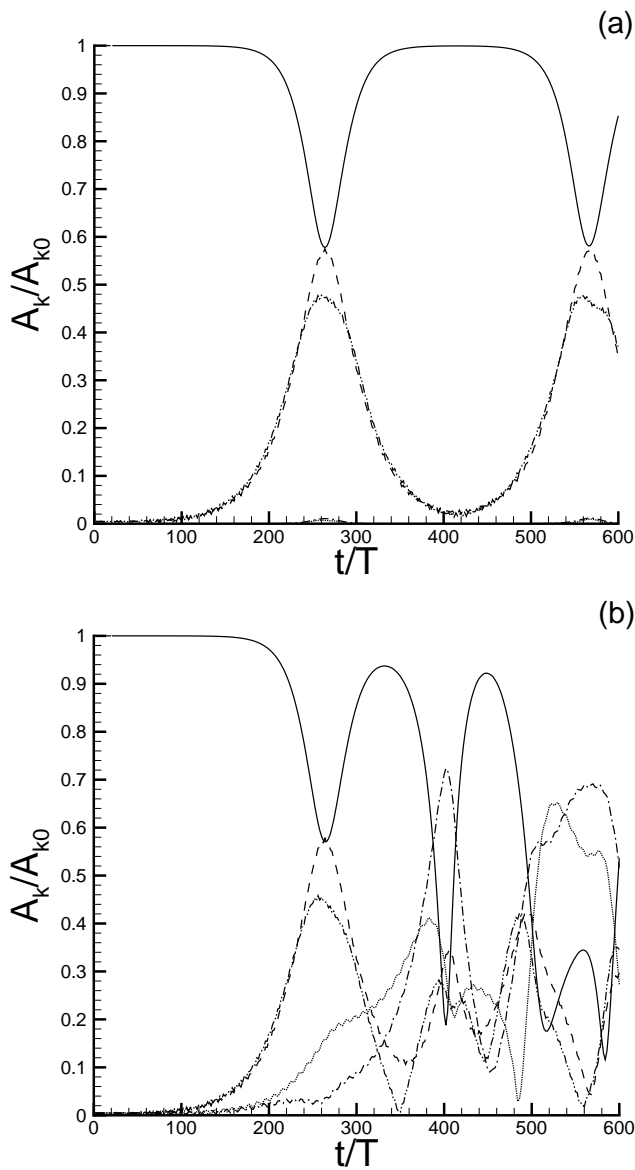


**Fig. 2.** Time evolution of the components of the fundamental mode  $k_0=9$  (solid line), of subharmonic modes  $k_1=7$  (dashed line) and  $k_3=8$  (dotted line), and of superharmonic modes  $k_4=10$  (dash-dotted line) and  $k_2=11$  (dash-dot-dotted line) propagated without wind. (a): From initial condition (1). (b): From initial condition (2).

In all simulations, the order of nonlinearity is taken such that  $M=8$ . The number of mesh points satisfies the condition  $N > (M + 1)k_{\max}$  where  $k_{\max}$  is the highest wavenumber taken into account in the simulation. Here, it has been taken equal to  $k_{\max}=70$ , and  $N=k_0 \times 100=900$ , so that 7 harmonics of the fundamental wavenumber are described. The latter criterion concerning  $N$  is introduced to avoid aliasing errors. More details concerning  $N$  is introduced to avoid aliasing errors. To compute the long time evolution of the wave packet the time step  $\Delta t$  is chosen equal to  $T/100$  where  $T$  is the fundamental period

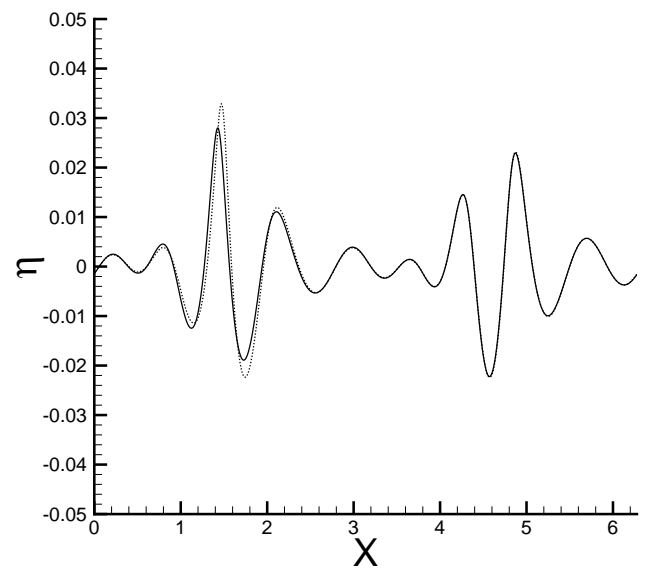


**Fig. 3.** Free surface elevation obtained at time  $t/T=280$ , from initial condition (2), without wind (solid line), and under wind action (dotted line).

of the basic wave. This temporal discretization satisfies the Courant-Friedricks-Lewy (CFL) condition of stability of finite difference scheme. Thus, a special concern regarding the accuracy of the method has been observed, since HOSM methods are known for the decay of accuracy for the steepest waves of concern here.

## 4 Results

### 4.1 Propagation without wind

Results obtained for both initial conditions propagated without wind are presented here. Figure 2 describes the normalized time evolution of the fundamental wavenumber  $k_0$  of the wave field, and sidebands of the two perturbations  $k_1, k_2, k_3$  and  $k_4$ .

On Fig. 2a, one can see the Fermi-Pasta-Ulam recurrence obtained from initial condition (1). The perturbation  $p$ , which is alone in this initial condition, passes through a maximum of modulation, during which components  $k_1$  and  $k_2$  are predominant. Then it demodulates, and the fundamental  $k_0$  gets its initial amplitude back. Afterward begins a new cycle. It is interesting to notice that the components involved in the process are  $k_0, k_1$  and  $k_2$ . The amplitude of components  $k_3$  and  $k_4$  remains almost constant through the modulation-demodulation cycle.

On Fig. 2b, it appears that no cycle is observed. This is understood since two perturbations are present in initial condition (2). As a matter of fact, two cycles are superimposed, and there is a nonlinear interaction of the components of each perturbation. It results in the destruction of the recurrence of

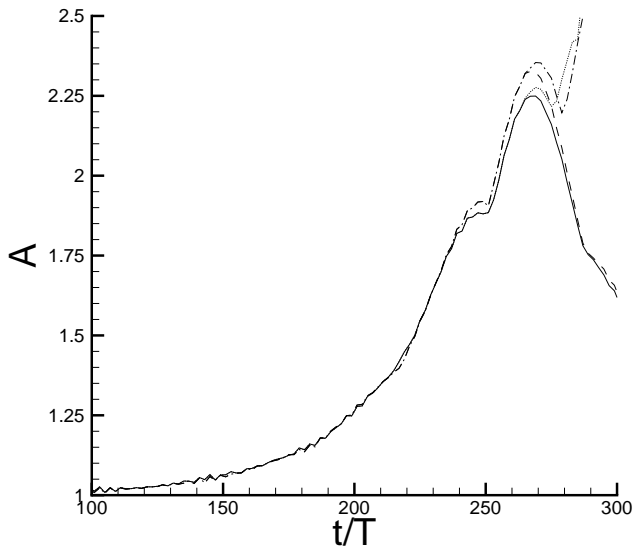


**Fig. 4.** Time evolution of the amplification factor  $A$ , obtained from: initial condition (1) without wind (solid line), initial condition (2) without wind (dashed line), initial condition (1) under wind action (dotted line), and initial condition (2) under wind action (dash-dotted line).

each cycle, and a more chaotic behavior. During some modulation, components  $k_1$  and  $k_2$  are predominant, while during some others, components  $k_3$  and  $k_4$  are.

#### 4.2 Propagation with wind

Initial conditions are now propagated under wind action. Figure 3 displays free surface elevations obtained from initial condition (2), propagated with and without wind for non-dimensional time  $t/T=280$ . This time corresponds barely to the maximum of modulation. It is interesting to notice that the height  $H$  of the wave propagated under wind action is larger than the height of the freak wave obtained without wind. But phase of the two waves remain very close. Phase velocity is almost not affected by the presence of wind.

From the height  $H$  of the waves, one can define an amplification factor  $A = \frac{H}{H_0}$ ,  $H_0$  being the wave height of the initial condition. Figure 4 displays the time evolution of this amplification factor for initial conditions (1) and (2), propagated with, and without wind. It is clear that in both cases, the presence of wind leads to an amplification of the freak wave. Furthermore, the time during which the wave group fulfills the freak wave criterion ( $\frac{H}{H_0} > 2$ ) is increased. This is understood as an increase of the freak wave's lifetime.

Simulations of the evolution of both initial conditions propagated under wind action stop around  $t/T=295$ . Numerical blow up appearing is understood as wave breaking, due to the large input of energy under wind action.

Figure 5 presents the evolution of components  $k_0$ ,  $k_1$ ,  $k_2$ ,  $k_3$  and  $k_4$  propagated under wind action, in the same way

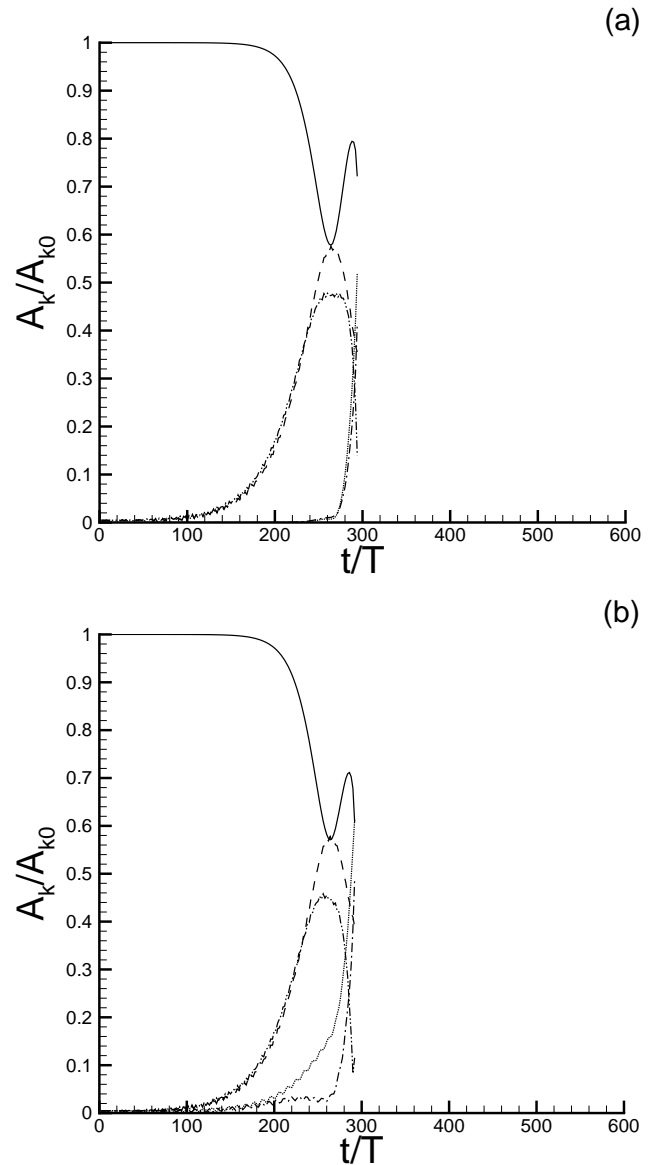


**Fig. 5.** Time evolution of the components of the fundamental mode  $k_0=9$  (solid line), of subharmonic modes  $k_1=7$  (dashed line) and  $k_3=8$  (dotted line), and of superharmonic modes  $k_4=10$  (dash-dotted line) and  $k_2=11$  (dash-dot-dotted line) propagated under wind action. **(a):** From initial condition (1). **(b):** From initial condition (2).

it was done on Fig. 2 without wind. Curves last up to  $t/T=295$ , after numerical blow up. Results obtained from initial conditions (1) and (2) are very similar. One can notice that in both cases, components  $k_1$  and  $k_2$  are not affected by the introduction of wind. Differences appear on the behavior of components  $k_3$  and  $k_4$ . If components related to perturbation  $p$  seem to follow the evolution they had without wind, components related to perturbation  $q$  show a rapid divergence from their behavior without wind. By comparing Fig. 2b and Fig. 5b, it appears that amplitude of the

components  $k_3$  and  $k_4$  grow earlier in presence of wind. In presence of wind, these components are dominant around  $t/T=290$ , while without wind, they are not dominant before  $t/T=400$ . Between Figs. 2a and 5a, the difference is also very important. The normalized amplitude of components  $k_3$  and  $k_4$ , related to perturbation  $q$ , never exceeds 0.01 when propagated without wind. But while propagated under wind action, these components become dominant after  $t/T=290$ . As a matter of fact, the modulation  $q$ , which is not the most unstable, turns out to be more sensitive to wind forcing. This observation could be explained while noticing that a phase opposition exists between the two freak waves present around the time of maximum modulation. Therefore, the forcing criterion is not overcome simultaneously, but alternatively by these waves. This could result in the forcing of the perturbation  $q$ , which presents one wavelength in the computational domain, instead of perturbation  $p$ , which presents two.

## 5 Conclusions

The effect of wind on freak waves generated by means of modulational instability has been investigated numerically. Two initial conditions have been considered. In the first one, only the most linearly unstable perturbation has been considered, while in the other one, the two perturbations linearly unstable were imposed. Those initial conditions have been propagated with, and without wind.

It appeared that without wind, the Fermi-Pasta-Ulam recurrence disappear when both modulations are present. This recurrence is broken by the presence of a second perturbation, of different growth rate. As a matter of fact, two cycle of different length are superimposed, and nonlinear interactions quickly destruct recurrence.

Under wind forcing, the lifetime of the freak wave is increased, in both cases. An amplification of the peak is also found, confirming previous results by Touboul and Kharif (2006). But in both cases, the influence of wind seems to help developing the perturbation which is not the most unstable. In both simulations, wind forcing lead to numerical blow up, which is understood as wave breaking.

As a result, it appears that wind blowing over rogue waves lead them to breaking. Those waves, naturally dangerous, become very more devastating while breaking. The impact of huge breaking waves on ships or off-shore structures is responsible of a large amount of energy destroying those structures. This phenomenon appears to be supported by wind action on rogue waves.

To improve and validate this approach, a stronger investigation of the pressure distribution in separating flows over waves is required. A two phase flow code is being developed for this study. A numerical simulation of the problem will provide a lot of information on the pressure distribution at the interface, and on the controlling parameters.

J. Touboul: On the influence of wind on extreme wave events

*Acknowledgements.* The author would like to thank C. Kharif for very interesting and helpful conversations.

Edited by: E. Pelinovsky

Reviewed by: two referees

## References

- Banner, M. I. and Melville, W. K.: On the separation of air flow over water waves, *J. Fluid Mech.*, 77, 825–842, 1976.
- Banner, M. I. and Tian, X.: On the separation of air flow over water waves, *J. Fluid Mech.*, 367, 107–137, 1998.
- Bliven, L. F., Huang, N. E., and Long, S. R.: Experimental study of the influence of wind on Benjamin-Feir sideband, *J. Fluid Mech.*, 162, 237–260, 1986.
- Dias, F. and Kharif, C.: Nonlinear gravity and capillary-gravity waves, *Annu. Rev. Fluid Mech.*, 31, 301–346, 1999.
- Dommermuth, D. and Yue, D.: A high order spectral method for the study of nonlinear water waves, *J. Fluid Mech.*, 184, 267–288, 1987.
- Giovanangeli, J. P., Touboul, J., and Kharif, C.: On the role of the Jeffreys' sheltering mechanism in sustaining extreme water waves, *C. R. Acad. Sci. Paris, Ser. IIB*, 8-9, 568–573, 2006.
- Jeffreys, H.: On the formation of wave by wind, *Proc. Roy. Soc. A*, 107, 189–206, 1925.
- Kharif, C. and Pelinovsky, E.: Physical mechanisms of the rogue wave phenomenon, *Eur. J. Mech. B/Fluids*, 22, 603–634, 2003.
- Kharif, C. and Ramamonjisoa, A.: Deep water gravity wave instabilities at large steepness, *Phys. Fluids*, 31, 1286–1288, 1988.
- Lawton, G.: Monsters of the deep (the perfect wave), *New Scientist*, 170(2297), 28–32, 2001.
- Longuet-Higgins, M. S.: Bifurcation in gravity waves, *J. Fluid Mech.*, 151, 457–475, 1985.
- Mallory, J. K.: Abnormal waves on the South-East Africa, *Int. Hydrog. Rev.*, 51, 89–129, 1974.
- McLean, J. W.: Instabilities of finite-amplitude water waves, *J. Fluid Mech.*, 114, 315–330, 1982.
- McLean, J. W., Ma, Y. C., Martin, D. U., Saffman, P. G., and Yuen, H. C.: Three-dimensional instability of finite-amplitude water waves, *Phys. Rev. Lett.*, 46, 817–820, 1981.
- Skandrani, C., Kharif, C., and Poitevin, J.: Nonlinear evolution of water surface waves: The frequency downshifting phenomenon, *Contemp. Math.*, 200, 157–171, 1996.
- Tanaka, M.: A method for studying nonlinear random field of surface gravity waves by direct numerical simulation, *Fluid Dyn. Res.*, 28, 41–60, 2001.
- Touboul, J. and Kharif, C.: On the interaction of wind and extreme gravity waves due to modulational instability, *Phys. Fluids*, 18, 108103, 2006.
- Touboul, J., Giovanangeli, J. P., Kharif, C., and Pelinovsky, E.: Freak waves under the action of wind: experiments and simulations, *Eur. J. Mech. B/Fluids*, 25, 662–676, 2006.
- Trulsen, K. and Dysthe, K. B.: Action of wind stress and breaking on the evolution of a wave train, in: *IUTAM Symposium on Breaking Waves*, edited by: Grimshaw, B., pp. 243–249, Springer-Verlag, 1991.
- West, B., Brueckner, K., Janda, R., Milder, M., and Milton, R.: A new numerical method for surface hydrodynamics, *J. Geophys. Res.*, 92(C11), 11 803–11 824, 1987.